Lecture Notes in Electrical Engineering 278

Aly A. Farag
Jian Yang
Feng Jiao
Editors

Proceedings of the 3rd International Conference on Multimedia Technology (ICMT 2013)

Springer

Lecture Notes in Electrical Engineering

Volume 278

For further volumes:
http://www.springer.com/series/7818

Aly A. Farag · Jian Yang · Feng Jiao
Editors

Proceedings of the 3rd International Conference on Multimedia Technology (ICMT 2013)

Springer

Editors
Aly A. Farag
Electrical and Computer Engineering
University of Louisville
Kentucky, KY
USA

Feng Jiao
Nanjing University of Information Science and Technology
Nanjing
People's Republic of China

Jian Yang
Department of Electronic Engineering
Tsinghua University
Beijing
People's Republic of China

ISSN 1876-1100 ISSN 1876-1119 (electronic)
ISBN 978-3-642-41406-0 ISBN 978-3-642-41407-7 (eBook)
DOI 10.1007/978-3-642-41407-7
Springer Heidelberg New York Dordrecht London

Library of Congress Control Number: 2013951133

Printed on acid-free paper

Springer is part of Springer Science+Business Media (www.springer.com)

Organizing Committee

General Chair

Prof. Aly A. Farag	Professor of University of Louisville, USA
Prof. Rangding Wang	Executive Dean, Ningbo Institutes of Advanced Technology, China

Technical Program Committee Chair

Prof. Jian Yang	Tsinghua University, China
Prof. Naixue Xiong, Ph.D.	School of Computer Science, Colorado Technical University, USA

Publication Chair

Jiao Feng, Ph.D.	Nanjing University of Information Science and Technology, China

Technical Program Committee

Wenyu Liu	Huazhong University of Science and Technology, China
Mingyan Jiang	Shandong University, China
Bo Sun	Beijing Normal University, China
Aiguo Song	Southeast University, China
Canhui Cai	Huaqiao University, China
Yougang Yang	Northwest A&F University, China
Chenglin Zhao	Shaoyang University, China
Chuanhe Huang	Wuhan University, China

Xianglin Huang	Communication University of China, China
Guiping Liao	Hunan Agricultural University, China
Junying Gan	Wuyi University, China
Feng Liang	Zhejiang Wanli University, China
Xiangyang Xue	Fudan University, China
Wei Xu	Jilin Agricultural Science and Technology College, China
Xun Wang	Zhejiang Gongshang University, China
Daifeng Zha	Jiujiang University, China
Fernando Ferri	IRPPS, CNR, Roma
Shashikant Patil	SVKM'S Nmims University, India
Yong BIAN	Canada Center for Remote Sensing, Natural Resources Canada, Canada
Xiaofei ZHANG	Nanjing University of Aeronautics and Astronautics, China
LV Teng	Army Officer Academy, China
Chuanrong ZHANG	University of Connecticut, USA
VPS Naidu	National Aerospace Laboratories, India
Francesco Zirilli	Universita di Roma La Sapienza, Italy
LI Bingzhao	Beijing Institute of Technology, China
Sukumar Senthilkumar	Chon Buk National University, Korea
Rajkumar Kannan	Bishop Heber College, India
Bormin Huang	University of Wisconsin-Madison, USA
Jian WANG	Cyber Physical System R&D Center, The Third Research Institute of Ministry of Public Security, China
Aniruddha Bhattacharjya	Amrita Vishwa Vidyappeetham University, India

Contents

Chapter 1
Spherical Mirror Estimation Using Phase Retrieval Wavefront Sensor Technology

Xinxue Ma, Jianli Wang, Bin Wang and Tianyu Lv

Abstract In order to verify the estimated wavefront ability of the phase retrieval wavefront sensor (PRWS), a measured spherical mirror of experiment platform was set up with the method of PRWS. PRWS technology is based on the focal plane image information wavefront solver in the focal plane wavefront measured technology, whose principle is sampling a number of the given defocus images; get the wavefront phase information by solving the optical system wavefront with Fourier optical diffractive theory and mathematics optimization. In order to validate the veracity of PRWS, both the PRWS measurement results and ZYGO interferometer measurement results were compared, experimental results demonstrate that agreement is obtained among the errors distribution, PV value and RMS value of ZYGO interferometer, so PRWS technology can effectively estimate the aberrations of spherical mirror.

Keywords Phase retrieval · Wavefront sensor · Spherical mirror · Zernike polynomial · Aberration

1.1 Introduction

In the machining processing of large-scale optics mirror in situ real-time estimation and alignment with the use of the optical system during dynamic measurement of wave aberrations is difficult to accomplish for the present tradition optical

X. Ma · J. Wang · B. Wang (✉) · T. Lv
Changchun Institute of Optics, Fine Mechanics and Physics, Chinese Academy of Sciences, Changchun 130033, China
e-mail: eatingbeen@hotmail.com

X. Ma
University of Chinese Academy of Sciences, Beijing 100039, China

A. A. Farag et al. (eds.), *Proceedings of the 3rd International Conference on Multimedia Technology (ICMT 2013)*, Lecture Notes in Electrical Engineering 278,
DOI: 10.1007/978-3-642-41407-7_1,

inspection equipment [1–3]. In order to control the optical quality of the telescope, we need a simple and with high accuracy method. This article proposed phase retrieval wavefront sensor (PRWS) technology [4–8] based on the focal plane image information wavefront solver in the focal plane estimated wavefront technology, whose principle is given by sampling a number of the defocus images [9–14]; solve the optical system wavefront by Fourier optical methods. System hardware is simple, free from the environment (especially the vibration) influence of optical components and systems for dynamic estimation, real-time display of measurements [7, 15], which has good application prospects in the field of the optical processing, system alignment, active optics, adapt optics etc.

In order to verify the estimated wavefront ability of PRWS, this paper set up a measured spherical mirror of experiment platform with the method of PRWS based on phase retrieval (PR) theory research and experimental verification. This paper compared PRWS measurement results with ZYGO interferometer [16–22] measurement results, experimental results demonstrate that agreement is obtained among the errors distribution, PV value and RMS value of ZYGO interferometer, so using PRWS technology can effectively test the spherical mirror aberration, which illustrates the feasibility and accuracy of PRWS measurement methods.

This paper is organized as follows: the theory of PRWS is presented in Sect. 1.2, the design of experiment in Sect. 1.3 and the summary in Sect. 1.4.

1.2 The Principles of PRWS

PR system is the wavefront detector of a focal plane waves; a laser spot light on the object plane is a target designated from the focal plane image acquisition, use the acquired image, the defocus of the corresponding image, known pupil size and shape to reverse solve the aberration of the optical system [23]. The structure of the PR system is shown in Fig. 1.1.

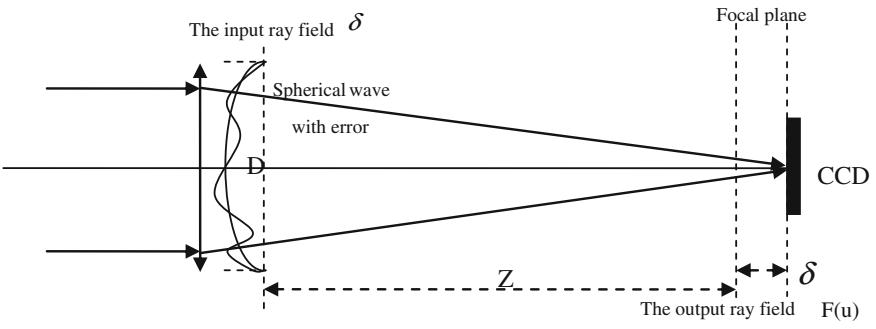

Fig. 1.1 Schematic of optical path of PR

Assuming that the aperture of a measured optical system is D, the focal length is Z, the center wavelength of the laser light source is λ, whose pupil constraint function is $|f(x)|$, the generalized pupil function for focus plane is

$$f(x) \quad = \quad |f(x)| \ \exp\left[i\theta(x)\right], \tag{1.1}$$

where θ is wavefront distortion and can be obtained with Zernike polynomial fitting: $\theta(x) = \sum_n \alpha_n Z_n(x)$, the real number α_n represents the first nth terms of polynomial coefficients, Z_n indicates the first nth terms of Zernike polynomials basement.

For linear optical system, when the generalized pupil $f(x)$ whose defocus is δ in the plane, the impulse response function $F(u)$ is

$$F(u) = |F(u)| \ \exp\left[i\psi(u)\right] = \mathcal{F}\{f(x) \ \exp\left[\varepsilon(x,\delta)\right]\}, \tag{1.2}$$

where x is the coordinates of the pupil domain, u is the coordinates of the image domain, both of them are two-dimensional vector field coordinates. ψ is the phase part of the impulse response, $\mathcal{F}$ is two-dimensional Fourier transform, $\varepsilon(x,\ \delta)$ is wavefront aberration caused by defocus δ in the position x.

For a PR system, $|f(x)|$ of Eq. (1.1) is the priori conditions of a known optical system, corresponds to the size and shape of the pupil. $|F(u)|^2$ is the image collected by CCD where the defocus is δ. Therefore, the purpose that we estimate wavefront by PR is to get α_n by the above known quantity. So formal description of the problem for: $|f(x)|,\ \delta_1, |F_1(u)|^2,\ \delta_2, |F_2(u)|^2, \ldots, \delta_M,\ |F_M(u)|^2$are known. Image acquisition distance from the focal plane at $\delta_1,\ \delta_2, \ldots, \delta_M$, respectively, is $|F_1(u)|^2,\ |F_2(u)|^2, \ldots,\ |F_M(u)|^2$.

The objective function and the partial derivative of PR objective function with respect to α_n, respectively, is Eqs. (1.3) and (1.4)

$$B_k = E_{Fk}^2 = N^{-2} \sum_{m=1}^{M} \sum_{u} \left[\left|G_{m,\,k}(u)\right| - |F(u)|\right]^2, \tag{1.3}$$

$$\partial_{a_n} B_k \ = \ -2 \sum_{m} \sum_{x} |f(x)| \left|g'_{m,k}(x)\right| \ \sin[\theta'_{m,k}(x) - \theta_{m,k}(x)] \ Z_n(x) \tag{1.4}$$

With the objective function (1.3) and its impact on the Zernike coefficient derivative (1.4), we can use the mathematical optimization algorithm to solve various Zernike wavefront coefficient values, here we use L-BFGS algorithm that the phase diversity (PD) [24–33] experiment has been able to solve. The following is solving steps:

Step 0 Selected starting point $\alpha^0 \in \mathcal{R}^n$ and the initial symmetric positive definite matrix $H_0 \in \mathcal{R}^{n\times n}$. Set the number of search accuracy ε bigger than zero and limited memory times m. Compute the gradient $\partial_\alpha B(\alpha^0)$, and order k is zero.

Step 1 If $\left\|\partial_{\alpha} B(\alpha^k)\right\| \leq \varepsilon$, the algorithm will terminate, the optimal solution is α^k,which is the wavefront Zernike coefficient. Otherwise, order d^k is $d^k = -H_k \partial_{\alpha} B(\alpha^k)$.

Step 2 Adopt the strategy of non-precise linear search, according to the Eqs. (1.3) and (1.4) determining step c_k, update $\alpha^{k+1}$is $\alpha^{k+1} = \alpha^k + c_k d^k$, and according to Eq. (1.4) for calculating the gradient values $\partial_{\alpha} B(\alpha^{k+1})$.

Step 3 Use the initial value H_0 or the intermediate information structure $H_k^{(0)}$, repeat using Eq. (1.5) for $m + 1$ times amending and get H_{k+1},

$$H_{k+1} = \left(I - \frac{s_k y_k^T}{s_k^T y_k}\right) H_k^{(0)} \left(I - \frac{y_k s_k^T}{s_k^T y_k}\right) + \frac{s_k s_k^T}{s_k^T y_k}, \tag{1.5}$$

where, $s_k = \alpha^{k+1} - \alpha^k$, $y_k = \partial_{\alpha} B(\alpha^{k+1}) - \partial_{\alpha} B(\alpha^k)$.

Step 4 Let $k = k + 1$, turn to Step 1. Where $\alpha = [\alpha_1, \ldots, \alpha_n]'$, α^k represents the value of α for k times iteration. In the L-BFGS algorithm, we only need to store $m + 1$ vector group $\{s_i, y_i\}_{i=k-m}^{k}$, and calculate the next iteration of the inverse of the Hessian matrix approximation. In practical calculation, usually select the appropriate m to control the amount of storage based on the problem of the size and machine performance. Generally the value of m ranges from 3 to 20, in this paper m is 5.

1.3 The Design of the Experiments

1.3.1 Experimental Theory and Components

The schematic diagram of PRWS is shown in Fig. 1.2. Gaussian beam emitted from the laser through the pinhole into a spherical wave, passes through the lens two into a parallel light, the light projects in the prism through the prism is divided into two parts, a part need not be considered, another part of the parallel reflects after a light through the lens 1 converge after the measured mirror, the reflected beam with phase information (i.e., aberration), again divided into two groups by a beam splitter, one part backtrack, the other part through the converging lens 3 converged at CCD camera, which is placed on a movable platform, move along the optical axis and the angle of the camera posture fine-tuning to get the focus before and after receiving a different amount of defocus images, used in realizing the estimated wavefront based on the PR. We can obtain aberration of the measured spherical mirror with the PR algorithm.

The focal length of measured spherical mirror is 0.2 m, the center wavelength is 632.5 nm, focal length of *3* in the experimental system is 0.15 m, the exit pupil caliber is 0.012 m, and the depth of focus is about 0.286 mm. In the experiment,

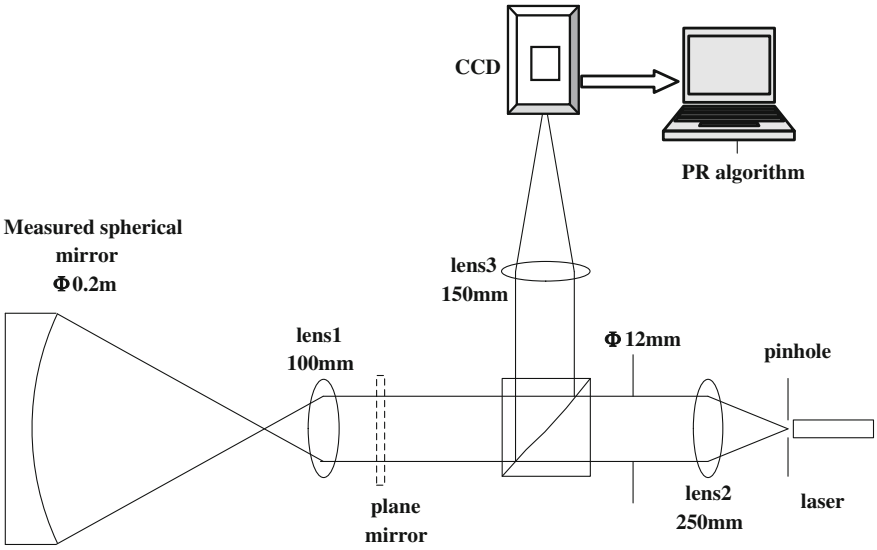

Fig. 1.2 Schematic diagram of PRWS

the defocus we select is 0, ±1, ±1.5, ±2 mm. Camera pixel size is 6.45 μm, each defocus position, respectively, intercept 128*128 pixel size of target region, the exposure time is 20 ms, the accuracy of mobile platform is ±5 μm. The experimental optical path is shown in Fig. 1.3.

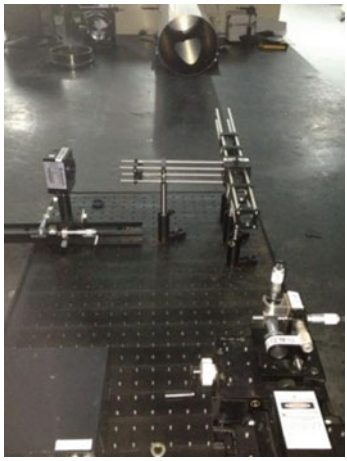

Fig. 1.3 The experimental system of PRWS

1.3.2 Experimental Procedures

In the process of the entire experimental, we not only prove the estimation ability of PRWS, but also prove the accuracy of PRWS, therefore during the experimental design, in order to ensure that the position of the measured spherical mirror during the whole experiment is invariable, we need to find the good distance between spherical mirror as shown in Fig. 1.4 with PRWS devices and between spherical mirror with ZYGO, respectively, based on the focal lengths of the measured spherical mirror. Then separately measure the spherical mirror with PRWS and ZYGO. Figure 1.5 is a diagram of the estimation experiment with the ZYGO interferometer.

1.3.3 Experimental Results and Discussion

We dispose the collected seven images with the PR algorithm, obtain the measured result of the spherical mirror is shown in Fig. 1.6. The measured result with the ZYGO interferometer is shown in Fig. 1.7.

In order to illustrate the accuracy and viability of the PRWS better, we rotated the spherical mirror a definite degree, and then estimate the spherical mirror with steps one to nine, the obtained measurement results are shown in Figs. 1.8 and 1.9.

In order to illustrate the accuracy and repeatability of PR, we rotated the spherical mirror some degree, and then estimate the spherical mirror with steps one to nine, the obtained measurement results are shown in Fig. 1.10.

Fig. 1.4 Tested telescope

Fig. 1.5 The experimental system of ZYGO interferometer measurement

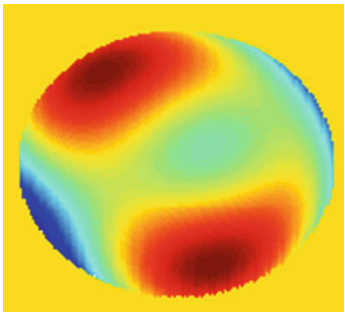

Fig. 1.6 Result of PRWS, RMS = 0.272λ, PV = 1.608λ

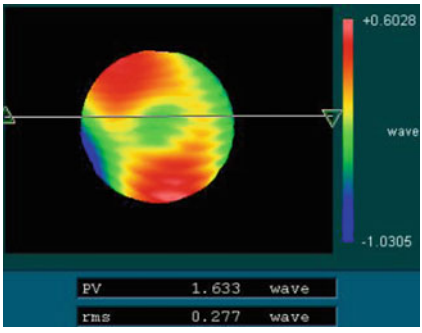

Fig. 1.7 Result of ZYGO interferometer, RMS = 0.277λ, PV = 1.633λ

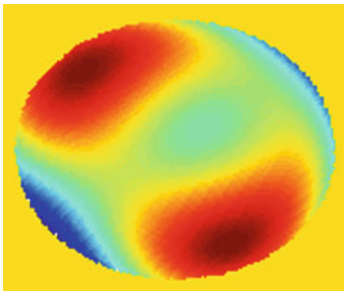

Fig. 1.8 Result of PRWS after rotation RMS = 0.280λ, PV = 1.501λ

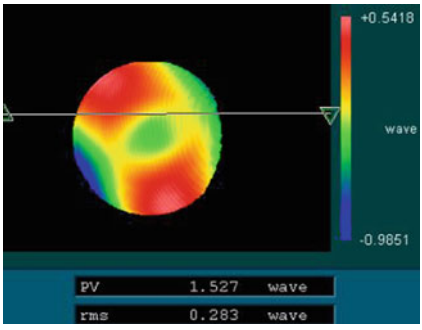

Fig. 1.9 Result of ZYGO interferometer after rotation, RMS = 0.283λ, PV = 1.527λ

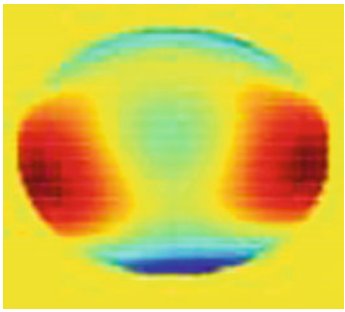

Fig. 1.10 Result of PR measurement after rotation, RMS = 0.271λ, PV = 1.659λ

From the measurement result after rotating, we can see that the results of estimated wavefront before and after rotation are agreement, and verify the PRWS measurement repeatability and effectiveness. Seeing from Figs. 1.6, 1.7, 1.8, and 1.9, for the same measurement mirror, the agreement is obtained among the errors distribution, PV value and RMS value of ZYGO interferometer, which explains the feasibility and accuracy of the PRWS measurement methods.

1.4 Conclusions

This paper set up an estimation spherical mirror of experiment platform with the method of PRWS, from the contrast of the measurement results before and after rotation, which verified the PRWS measurement repeatability and effectiveness. In order to validate the veracity of PRWS, this paper compared PRWS measurement results with ZYGO interferometer measurement results, experimental results demonstrate that agreement is obtained among the errors distribution, PV value and RMS value of ZYGO interferometer, so using PRWS technology can effectively estimate the spherical mirror aberration, which explains the feasibility and accuracy of the PRWS measurement methods, which provides the feasibility to data support for our later search.

References

1. Brown B, Aaron M (2001) The politics of nature. In: Smith J (ed) The rise of modern genomics, 3rd edn. Wiley, New York
2. Brady Gregory R, Fienup JR (2004) Improved optical metrology using phase retrieval. Optical fabrication and testing, vol 10. Rochester, NY, 2004, p 1–3
3. Yang H, Gong C (2011) Phase retrieval for a kind of wavefront sensor based on pupil phase diversity. Acta Optica Sinica 31(11):1112002
4. Osten W (2008) Some answers to new challenges in optical metrology. Proc SPIE 7155: 715503-1–715503-16

5. Ohara CM, Faust JA, Lowman AE et al (2004) Phase retrieval camera optical testing of the advanced mirror system demonstrator. SPIE 5487:1744–1756
6. Gerchberg RW, Saxton WO (1972) A practical algorithm for the determination of phase from image and diffraction phase pictures. Optic 35(2):237–246
7. Fienup JR (1982) Phase retrieval algorithms: a comparison. Appl Opt 21(15):2758–2769
8. Fienup JR, Marron JC, Schulz TJ et al (1993) Hubble space telescope characterized by using phase-retrieval algorithms. Appl Opt 32(10):1747–1767
9. Dean Bruce H, Aronstein David L, Smith JS et al (2006) Phase retrieval algorithm for JWST flight and testbed telescope. Proc SPIE 6265:1–17
10. Fei Li, Changhui Rao (2011) Study on phase diversity wavefront sensor. Acta Optica Sinica 31(8):0804001
11. Liang S, Yang J, Xue B (2010) A new phase diversity wave-front error sensing method based on genetic algorithm. Acta Optica Sinica 30(4):1015–1019
12. Jiang P, Ma H, Zou Y et al (2011) Study of aberration correction in light path of adaptive optical system. Acta Optica Sinica 31(12):1214002
13. Devaney AJ, Childlaw R (1978) On the uniqueness question in the problem of phase retrieval from intensity measurement. JOSA A 68(10):1352–1354
14. Han B, Xiao W, Pan F et al (2012) Optimization of space sampling distance of phase retrieval algorithm for in-line digital holography. Laser Optoelectron Prog 49:120903
15. Fu F, Bin Z (2011) Recovery of high frequency phase of laser beam with wavefront distortio. Chin J Lasers 38(4):0402009
16. Brady Gregory R, Fienup JR (2005) Phase retrieval as an optical metrology tool. In: Optical fabrication and testing. Topical meeting of the optical society of America, SPIE Technical Digest 2005, TD03, pp 139–141
17. Millerd JE, Wyant JC (2005) Simultaneous phase-shifting fizeau interferometer.US Patent 20050046864
18. Deck Leslie (1996) Vibration-resistant phase-shifting interferometry. Appl Opt 35(34):6655–6662
19. Burge JH, Wyant JC (1995) Applications of computer-generated holograms for interferometric measurement of large aspheric optics. Proc SPIE 2576:258–269
20. Reichelt S, Pruss C, Tiziani HJ (2003) Absolute interferometric test of aspheres by use of twin computer- generated holograms. Appl Opt 42(22):4468–4479
21. Sommargren GE, Phillion DW, Campbell EW (1999) Sub-nanometer interferometry for aspheric mirror fabrication. In:The 9th international conference on production engineering, Osaka, Japan, 1999
22. Reichelt S,Tiziani HJ (2003) Twin-CGHs for absolute calibration in wavefront testing interferometry. Opt Commun 220:23–32
23. Ma X, Wang J, Wang B (2012) Study on phase retrieval algorithm. Laser Infrared 42(2):217–221
24. Wang JL, Wang ZY, Wang B et al (2011) Image restoration by phase-diversity speckle. Opt Precis Eng 19(5):1165–1170
25. Wang B, Wang ZY, Wang JL et al (2011) Phase-diverse speckle imaging with two cameras. Opt Precis Eng 19(6):1384–1390
26. Zhao JY, Chen ZF, Wang B et al (2012) Improvement of phase diversity object function's parallelity. J Opt Precis Eng 20(2):431–438
27. Wang B, Ma XX et al (2013) Calibration of no-common path aberration in AO system using multi-channel phase-diversity wave-front sensing. Opt Precis Eng 21(7):1683–1692
28. Wang ZY, Wang B, Wu YH et al (2012) Calibration of non-common path static aberrations by using phase diversity technology. Acta Optica Sinica 32(7):0701007
29. Zhao JY, Ma XX et al (2012) Image restoration based on real time wave-front information. Opt Precis Eng 20 (6):1350–1356
30. Byrd RH, Lu P, Nocedal J (1995) A limited-memory algorithm for bound-constrained optimization. SIAM J Sci Stat Comput 16(5):1190–1208

31. Mahdi H, Stojan R et al (2012) Memory-enhanced noiseless cross-phase modulation. Light Sci Appl 40
32. Lingling H, Xianzhong C et al (2013) Helicity dependent directional surface plasmon polariton excitation using a metasurface with interfacial phase discontinuity. Light Sci Appl 2:e70
33. Dai D, Bauters J, Bowers JE (2012) Passive technologies for future large-scale photonic integrated circuits on silicon: polarization handling, light non-reciprocity and loss reduction. Light Sci Appl 1:e1

Chapter 2
Combined Utility and Adaptive Residence Time-Based Network Selection for 4G Wireless Networks

J. Shankar, C. Amali and B. Ramachandran

Abstract Next generation wireless networks are expected to include heterogeneous wireless networks to offer a diverse range of multimedia services to mobile users. Due to the heterogeneity and the diversity of access networks, various user applications with different Quality of Service (QoS) requirements pose new challenges on multi-interface Mobile Terminal (MT) in designing optimal network selection algorithm for guaranteeing seamless QoS support to the users. Thus, Vertical Hand Off (VHO) is necessary to provide uninterrupted services to mobile users anywhere and anytime in 4G networks. In this paper, Service continuity with guaranteed QoS and minimum VHO rate is considered as a challenging issue. In order to achieve this, discovered networks are evaluated periodically according to the velocity and direction of Mobile Terminal. Network evaluation is carried out through the integration of utility function calculation and cell residence time estimation. The proposed scheme avoids unnecessary VHO by selecting the network based on the capabilities of MT, QoS requirements of ongoing service and characteristics of networks. Thus, it eliminates the probability of HO failure by considering all possible critical factors and adaptive Residence Time (RT) threshold in 4G wireless networks. The results are compared against the performance of utility-based handoff and residence time-based handoff schemes. The simulation results show that the proposed scheme reduces the number of unnecessary handoffs which in turn minimizes the VHO rate and probability of HO failure in 4G wireless networks.

Keywords Vertical · Handoff · Heterogeneous network · Utility function · Adaptive residence time · QoS

J. Shankar (✉) · C. Amali · B. Ramachandran
SRM University, Chennai, India
e-mail: shankarjayaraj@hotmail.co.in

C. Amali
e-mail: amali.vec@gmail.com

B. Ramachandran
e-mail: ramachandran.b@ktr.srmuniv.ac.in

A. A. Farag et al. (eds.), *Proceedings of the 3rd International Conference on Multimedia Technology (ICMT 2013)*, Lecture Notes in Electrical Engineering 278,
DOI: 10.1007/978-3-642-41407-7_2,

2.1 Introduction

The future wireless and mobile environments are likely to have users to access multiple networks at the same time. In fourth generation (4G) wireless networks, users are able to roam freely from one type of wireless access network to another while preserving the main characteristics of their connections. Therefore, there is a need to have mechanisms to decide which network is the most suitable for each user at each moment for every application that the user requires. Vertical Hand Off (VHO) is the capability to switch on going connections from one Radio Access Network (RAN) to another. The trend is to utilize high bandwidth wireless local area network (WLAN) resource for mobile users in hotspots and switch to Cellular Networks (CN) when the coverage of WLAN is not available. The strength of 4G systems is to integrate existing and newly developed wireless systems instead of putting efforts in developing new radio interfaces and technologies to provide seamless mobility and better service quality for 4G users. In this paper, the coexistence of UMTS, WLAN, and WiMAX access networks are considered as a heterogeneous wireless network which is illustrated in Fig. 2.4. Hence, it is expected that mobile users could enjoy seamless mobility and ubiquitous service access in an always best connected mode, the development of an appropriate interworking solution for these heterogeneous wireless networks is crucial.

The criteria involved in VHO decision are very important to achieve uninterrupted mobility scenarios in taking decisions for switching to the target network from both application requirements and mobile terminal capabilities. The decision making process of handoff may be centralized or decentralized (i.e., the handoff decision may be made at the network or Mobile Terminal (MT)). From the decision process point of view, one can find at least three different kinds of handoff decisions. They are, (1) Network assisted handoff (2) Mobile assisted handoff and (3) Mobile controlled handoff. Out of these three, mobile controlled and network assisted handoff are combined to get Mobile Controlled Network Assisted (MCNA) handoff, because only the MT has the knowledge about the networks available in the coverage area.

If the mobile terminal velocity and moving pattern are irregular, more unnecessary handoff can occur. In our proposed algorithm, these two factors are considered as important parameters to select the target network in heterogeneous wireless networks. When the MT is moving with high velocity, it is necessary to find out how much time the MT will stay in the target network. If the estimated residence time is less than the predefined threshold, handoff to such a network is not beneficial as, it requires more number of handoff to complete the ongoing service.

The remainder of this paper is organized as follows: The related and existing works with their shortcomings are discussed in Sect. 2.2. The system model of the proposed scheme to improve the network selection mechanism is explained in Sect. 2.3. Section 2.4 presents the different modules of the proposed algorithm. The simulation environment and the results are discussed in Sect. 2.5. Finally, the paper is concluded with Sect. 2.6.

2.2 Related Work

Recently, various network selection algorithms based on Multiple Attribute Decision Making (MADM) approach have been developed to improve the VHO decision in heterogeneous wireless networks. An Analytic Hierarchy Process (AHP)-based network selection algorithm for UMTS and WLAN is presented in [1]. AHP and Grey Relational Analysis (GRA)-based network selection mechanism for UMTS and WLAN is presented in [2] for next generation networks. In [3], a fuzzy logic-based MADM problem is formulated in which multiple parameters are considered to perform VHO decision in heterogeneous networks. Fuzzy logic is used to represent the imprecise information of different parameters of the networks and the preferences of the user. The method for discovering the reachable wireless networks is proposed in [4] and it is the first step for VHO. After discovering the reachable candidate networks, the mobile terminal decides whether to perform handoff or not.

In [5], a Position Aware Vertical Handoff decision algorithm (PAHO) has been proposed which considers the MS's position, its moving pattern and speed and also the coverage area of the current BS to select the target network for performing VHO. In [6], a target network is selected by calculating a utility function which considers parameters such as available bandwidth, SINR, traffic load, and MS speed. In [7], a movement aware VHO algorithm is proposed to exploit the MT velocity and movement pattern for eliminating ping pong effects and reducing unnecessary handovers. The handoff decision is made based on the comparison of cost functions of different access networks [8]. In most existing cost function-based network selection algorithm, a set of network and user parameters are chosen as the cost factors and fixed weights are assigned in designing the cost function. As Next Generation Wireless Networks (NGWN) is expected to support users with different profiles and service applications with different Quality of Service (QoS) requirements, cost function with fixed weights cannot efficiently reflect the QoS requirements on communication service, resulting in low efficiency in network selection. Thus, in [9] a Modified Weight Function-based Network Selection Algorithm (MWF-NSA) that considers user preference and application profile has been proposed in deciding the weight functions of the networks. In [10], traveling distance prediction is used to perform handoff necessity estimation and also to avoid unnecessary handoffs from cellular network to WLAN.

In this paper, the discovered networks are preselected based on the velocity of MT. Utility function is calculated for evaluating the preselected networks. The network which has maximum utility function is considered for residence time estimation. Thus, our proposed work aims to incorporate the characteristics of networks, QoS requirements of different traffics, MT velocity, and moving pattern to select the best suitable network to perform VHO in heterogeneous wireless networks.

2.3 System Model of the Proposed Algorithm

The performance of the proposed algorithm is compared with utility-based and residence time-based VHO schemes. In utility-based VHO scheme, optimized utility function is used to select the target network by introducing trade-off between user satisfaction and network efficiency. Whereas, residence time-based VHO decision scheme estimates the traveling time of mobile terminal in the candidate networks using MT velocity and direction. In this scheme, time threshold value should be high for high velocity of MT in order to increase the resource utilization and also to provide uninterrupted services to mobile users.

In the proposed scheme, the above two approaches are combined and named as Combined Utility and Adaptive Residence Time (CU-ART)-based network selection algorithm which select the best network based on the capabilities of MT, network conditions, and QoS requirements of running applications. An appropriate system model is constructed to give the sequence of processes involved in the proposed algorithm. This model is then analyzed and simulated using utility function and mathematical techniques.

Figure 2.1 represents the system model of proposed CU-ART algorithm. New networks are discovered based on Received Signal Strength (RSS) measurements in a given coverage area. These newly discovered networks are filtered through a network preference block based on velocity of MT. Utility block finds the utility value of the networks in the filtered lists. The network which has maximum utility function is considered for residence time estimation. Residence time is the time for which the mobile terminal stays in the particular network. Longer the residence time lesser will be the frequency of handoffs. The network with residence time greater than the adaptive Residence time threshold is selected as a target network. Thus, the proposed system model not only satisfies the QoS requirements of mobile users but also improves the system performance by reducing the unnecessary VHO.

2.4 Working of CU-ART Network Selection Algorithm

The three modules of the proposed algorithm are, (1) Discovery and Preselection of networks (2) Utility function calculation and (3) Residence time estimation.

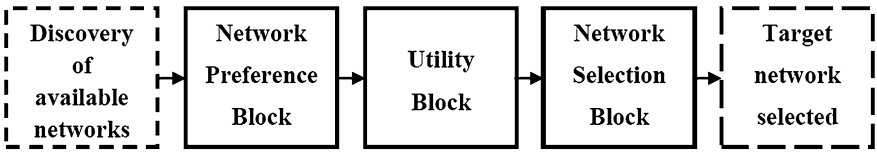

Fig. 2.1 System model

2.4.1 Discovery and Preselection of Networks

The networks available in the given coverage area are discovered by measuring the RSS from BS. The networks which have RSS greater than the threshold value are considered for preselection process. This module obtains the information about velocity and moving direction of MT from GPS system. Then, the discovered networks are preselected based on the speed that supports. Networks with low coverage cannot provide services to high speed mobile users. As a result, large number of handover is required to maintain the ongoing service. WLAN is capable of providing low mobility and high bandwidth services. But WiMAX and UMTS support applications which require large coverage area and medium bandwidth. By selecting the networks according to the MT velocity, number of VHO required to complete the ongoing connection can be minimized.

Figure 2.2 illustrates the working of proposed CU-ART-based network selection algorithm. The network preselection is done with respect to velocity of MT. Average pedestrian speed (i.e., 1.4 m/s) is considered to filter the discovered networks. Utility function is calculated only for filtered networks to reduce computation time which in turn minimizes the HO delay. The network with maximum utility and residence time greater than the adaptive residence time threshold is selected as a target network. It is explained further in the following subsections.

2.4.2 Utility Function Calculation

The Utility module reads the network parameters such as bandwidth, connection delay, and cost whenever networks are discovered. To support user applications with different levels of QoS requirements, 3GPP has defined four traffic classes such as Conversational class, Streaming class, Interactive class, and Background class. The characteristics of different traffics must be taken into account in the design of network selection algorithm in order to provide better performance to the users in the integrated networks. Appropriate weight factor should be assigned to each metric to account for its importance in providing QoS requirements to particular application. The importance levels of High, Medium, and Low for a particular parameter 'i' is defined as i_H, i_M, and i_L, respectively. They are in the order $0 < i_L < i_M < i_H < 1$. The values assumed are $i_L = 0.3$, $i_M = 0.6$ and $i_H = 0.9$. The weight factors of the importance levels are W_H, W_M, and W_L, respectively, where $W_H + W_M + W_L = 1$.

$$W_L = \frac{i_L}{(i_H + i_M + i_L)}, \quad W_M = \frac{i_M}{(i_H + i_M + i_L)}, \quad W_H = \frac{i_H}{(i_H + i_M + i_L)}$$

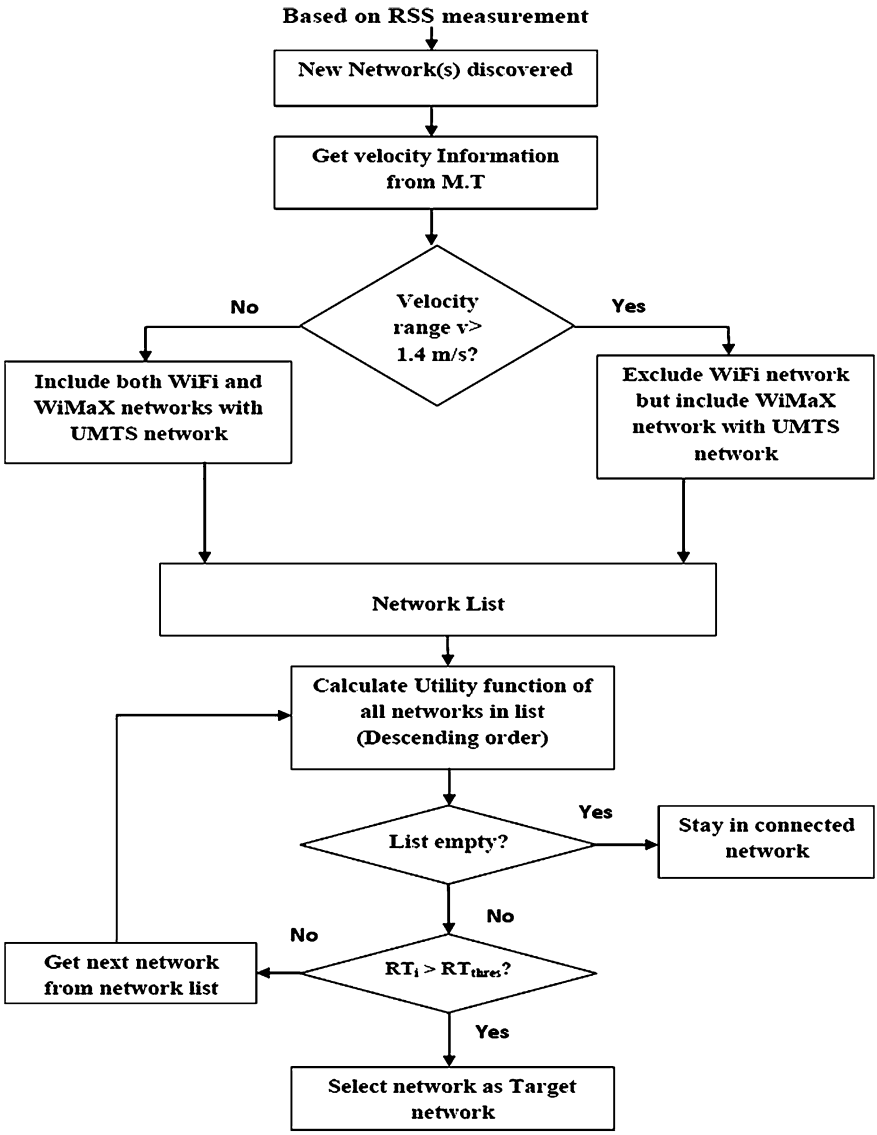

Fig. 2.2 Flowchart of CU-ART algorithm

W_H, W_M, and W_L are high medium and low weights respectively. Then, utility function is calculated for the integration of Wi-Fi, UMTS, and WiMAX based on the network conditions and QoS requirements of ongoing service.

The utility function is calculated using the following formulae given in [9].

$$\mathrm{NEF}_j = W_D\left(1 - D_j\right) + W_B B_j + W_C\left(1 - C_j\right)$$

Table 2.1 Utility values of networks

Application types	Utility values					
	For velocity < 1.4 m/s			For velocity >=1.4 m/s		
	Wi-Fi	UMTS	WiMAX	Wi-Fi	UMTS	WiMAX
Video call	0.388893	0.333322	0.277785	0	0.54544	0.45456
Voice call	0.388887	0.333322	0.277791	0	0.545435	0.454565
FTP	0.4	0.33332	0.26668	0	0.555533	0.444467
Video Stream	0.388887	0.333322	0.277791	0	0.545435	0.454565
Browsing	0.388887	0.333322	0.277791	0	0.545435	0.454565
Messaging	0.388887	0.333322	0.277791	0	0.545435	0.454565
Navigation Application	0.388893	0.333322	0.277785	0	0.54544	0.45456
Gaming	0.375	0.333325	0.291675	0	0.53332	0.46668

where j corresponds to Wi-Fi, UMTS, and WiMAX and W_D, W_B, and W_C are weights for delay, bandwidth, and cost respectively. They are calculated according to the QoS requirements of applications for each network which are shown in Table 2.1. Application types that are considered in this algorithm are (1) Video call (2) Voice call (3) FTP (4) Video Stream (5) Browsing (6) Messaging (7) Navigation Application and (8) Gaming. The numerical results of utility function module for different applications are shown in Table 2.1 based on the velocity of MT. From the table, it is inferred that for MT moving with velocity greater than 1.4 m/s (average pedestrian speed), utility function is available only for UMTS and WiMAX to serve the mobile users with minimum VHO frequency.

2.4.3 Residence Time Estimation

In order to minimize the probability of HO failures and unnecessary HO, residence time is estimated for the networks available in the given direction of MT. The network with maximum residence time is selected to serve the mobile users. Figure 2.3 illustrates the residence time calculation using trigonometric method. P_1 and P_2 are arbitrary points on the boundary through which MT enters into the network from which the value of θ is determined. The value of θ is uniformly distributed in $[0, 2\pi]$.

2.4.3.1 Residence Time (t)

Residence time of MT is estimated by using the parameters such as direction (θ), velocity (v), and the radius of network coverage (R).

In Fig. 2.3, considering right angle triangle OAP_1.

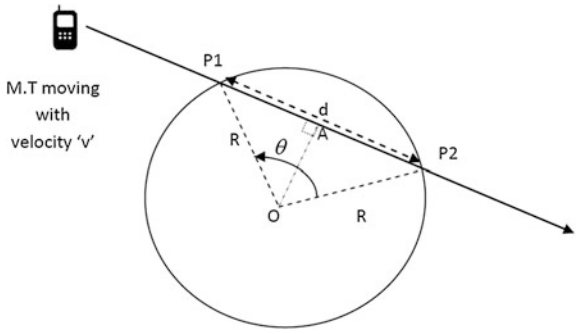

Fig. 2.3 Scenario for residence time estimation

$$\sin {}^{\theta}/_{2} = \frac{{}^{d}/_{2}}{R} \quad \text{Squaring on both sides gives}$$

$$\sin^2 {}^{\theta}/_{2} = \frac{d^2}{4R^2} \text{ leads to } \quad \frac{(1-\cos\theta)}{2} = \frac{d^2}{4R^2}$$

where d is the distance between P_1 and P_2 and θ is the angle between points P_1 and P_2 with respect to base station.

From $d = v_{*}t$, the residence time of MT can be expressed as:

$$t = \sqrt{\frac{2R^2(1-\cos\theta)}{v^2}} \tag{2.1}$$

2.4.3.2 Adaptive Residence Time Threshold (T)

Adaptive residence time threshold is needed for high speed users to reduce the HO failure probability and HO frequency. From Eq. 2.1, it is known that the estimated RT is a function of θ, v, and R. In the given scenario, more number of trajectories can be generated by considering different values of θ for the evaluation of discovered networks. For $\theta = 0^{\circ}$, the point P_1 and P_2 coincide and path of MT just graces through the boundary. For this case, the estimated RT is zero. For $\theta = 180^{\circ}$, the path of the MT goes through the diameter of network coverage offering maximum residence time.

Using the theorem stated in [10], the pdf of estimated RT is given by:

$$f(T) = \begin{cases} \frac{2}{\pi\sqrt{4R^2 - v^2T^2}}; & 0 \le T < \frac{2R}{v} \\ 0; & \text{Otherwise} \end{cases} \tag{2.2}$$

The Eq. 2.2 is evaluated to obtain the pdf for different velocities.

$$f_{\text{mean}}(T) = \text{mean}(f(T)) \quad \forall \quad 1 < T < T_{\max} \tag{2.3}$$

$T_{\max}$ for Wi-Fi, UMTS, and WiMAX is 12 s, 160 s, 400 s, respectively. It is calculated based on the typical network radius of 150 m, 2000 m, and 5000 m, respectively.

Mean of pdf is considered from worst case estimated residence time of 1 s to maximum limit ($T_{\max}$).

From Eq. 2.2, the adaptive residence time threshold is given by:

$$T = \frac{1}{v}\sqrt{\left(4R^2 - \frac{4}{\pi^2(f(T))^2}\right)} \tag{2.4}$$

From Eqs. 2.3 and 2.4,

$$T = \frac{1}{v}\sqrt{\left(4R^2 - \frac{4}{\pi^2(f_{\text{mean}}(T))^2}\right)} \tag{2.5}$$

The adaptive RT threshold for a particular velocity is calculated using Eq. 2.5. Where, v is velocity of MT, R is radius of network, $f_{mean}(T)$ is the mean pdf value of RT evaluated under $\frac{2R}{v}$.

2.4.3.3 Probability of Handoff (P_{HO})

Handoff occurs when estimated RT of MT is greater than the adaptive residence time threshold T. The probability of handoff to occur can be evaluated from the cdf of estimated RT which is obtained by integrating the pdf in Eq. 2.2.

$$\begin{aligned} P_{\text{HO}} &= F(T) = P(t \geq T) \\ P_{\text{HO}} &= \int_{T}^{\infty} f(T)dT \\ &= \begin{cases} 1 - \frac{2}{\pi}\arccos\left(\frac{vT}{2R}\right) & ; \quad 0 \leq T \leq \frac{2R}{v} \\ 0 & ; \quad \text{otherwise} \end{cases} \end{aligned} \tag{2.6}$$

The probability of handoff occurrence is given by Eq. 2.6 for the networks available in the direction of MT moving with a velocity 'v'.

2.5 Simulation Results and Discussion

The three modules of proposed CU-ART algorithm are simulated using Matlab. The network coverage radius for Wi-Fi, UMTS, and WiMAX is assumed as 150, 2000, and 5000 m, respectively. The heterogeneous scenario used for simulation is

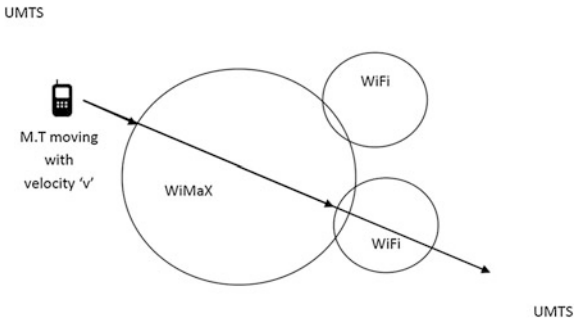

Fig. 2.4 Heterogeneous scenario

shown in Fig. 2.4. In this scenario, it is assumed that UMTS network covers the entire area because of widely deployed 3G network.

2.5.1 Residence Time

Residence time of MT across the Wi-Fi network for different random trajectories (θ) obtained through simulation is shown in Fig. 2.5 with respect to the velocity of the MT. Five different values of θ are considered (i.e., $\theta = 0°, 30°, 60°, 90°, 180°$) for simulation. The estimated residence time of MT across the Wi-Fi network is shown in Fig. 2.5 which shows the effect of velocity and moving direction on residence time estimation. From simulation, it is also found that the estimated residence time values for UMTS and WiMAX are 400 and 2000 s respectively for a particular velocity of 5 m/s with $\theta = 60°$.

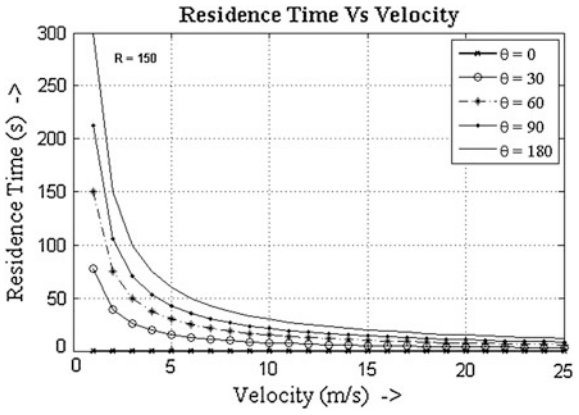

Fig. 2.5 Residence time for Wi-Fi network